Complex dewetting scenarios captured by thin-film models

JÜRGEN BECKER[1], GÜNTHER GRÜN[1], RALF SEEMANN[2], HUBERT MANTZ[2], KARIN JACOBS[2], KLAUS R. MECKE[3,4] AND RALF BLOSSEY*[5]

[1]Institut für Angewandte Mathematik, Universität Bonn, Beringstrasse 6, D-53115 Bonn, Germany
[2]Abteilung Angewandte Physik, Universität Ulm, D-89069 Ulm, Germany
[3]Max-Planck-Institut für Metallforschung, Heisenbergstrasse 1, D-70569 Stuttgart
[4]Institut für Theoretische und Angewandte Physik, Universität Stuttgart, Pfaffenwaldring 57/VI, D-70550 Stuttgart, Germany
[5]Zentrum für Bioinformatik, Universität des Saarlandes, Im Stadtwald, D-66123 Saarbrücken, Germany
*e-mail: blossey@bioinf.uni-sb.de

Published online: 15 December 2002; doi:10.1038/nmat788

In the course of miniaturization of electronic and microfluidic devices, reliable predictions of the stability of ultrathin films have a strategic role for design purposes. Consequently, efficient computational techniques that allow for a direct comparison with experiment become increasingly important. Here we demonstrate, for the first time, that the full complex spatial and temporal evolution of the rupture of ultrathin films can be modelled in quantitative agreement with experiment. We accomplish this by combining highly controlled experiments on different film-rupture patterns with computer simulations using novel numerical schemes for thin-film equations. For the quantitative comparison of the pattern evolution in both experiment and simulation we introduce a novel pattern analysis method based on Minkowski measures. Our results are fundamental for the development of efficient tools capable of describing essential aspects of thin-film flow in technical systems.

The thickness of, for example, insulating layers or photo resists for the fabrication of electronic chips now reaches the order of a few nanometres, resulting in new challenges for guaranteeing stability during production and use of the device[1]. In an experimental model system, a thin polystyrene (PS) film on a Si wafer, we have established stability criteria for the thin film that take into account the thickness of the SiO layer on top of the Si wafer and the thickness h of the PS film. The free energy $\mathcal{H}$ of this system is given by the expression

$$\mathcal{H}[h] = \int \mathrm{d}\vec{x} \left[\frac{\sigma}{2} (\nabla h)^2 + V(h) \right] \qquad (1)$$

where $\vec{x}$ denotes a spatial point within a two-dimensional substrate Ω. This expression comprises a long-wavelength approximation for the capillary energy with surface tension σ and $V(h)$ as an effective interface potential that covers intermolecular forces beyond capillarity. An analysis of the evolving structures allowed insight into the underlying forces of the system[2]. Thus, given sufficient knowledge of system parameters (such as dielectric constants of the participating media), the principal question of stability or instability of a given thin film can now be answered.

This knowledge, however, is not sufficient to enable understanding of the evolution of the instability of a thin film. As simulations based on molecular dynamics are still too complex numerically, the theoretical framework for the description of fluid flow is based on approaches from continuum mechanics[3,4]. In the case of interest here, the viscosity of the liquid and the disparity between horizontal and vertical lengthscales permit the associated free-surface problem for the Navier–Stokes equations to be replaced by a dimension-reduced free-boundary problem of lower complexity. This is accomplished along the lines of a lubrication approximation, and leads to a fourth-order degenerate diffusion equation for the film height $h(\vec{x}, t)$ above Ω, involving singular terms of second order[4]. Energy is dissipated solely due to viscous friction, and scaling arguments performed in the framework of the Navier–Stokes equations indicate that the horizontal flow profile is

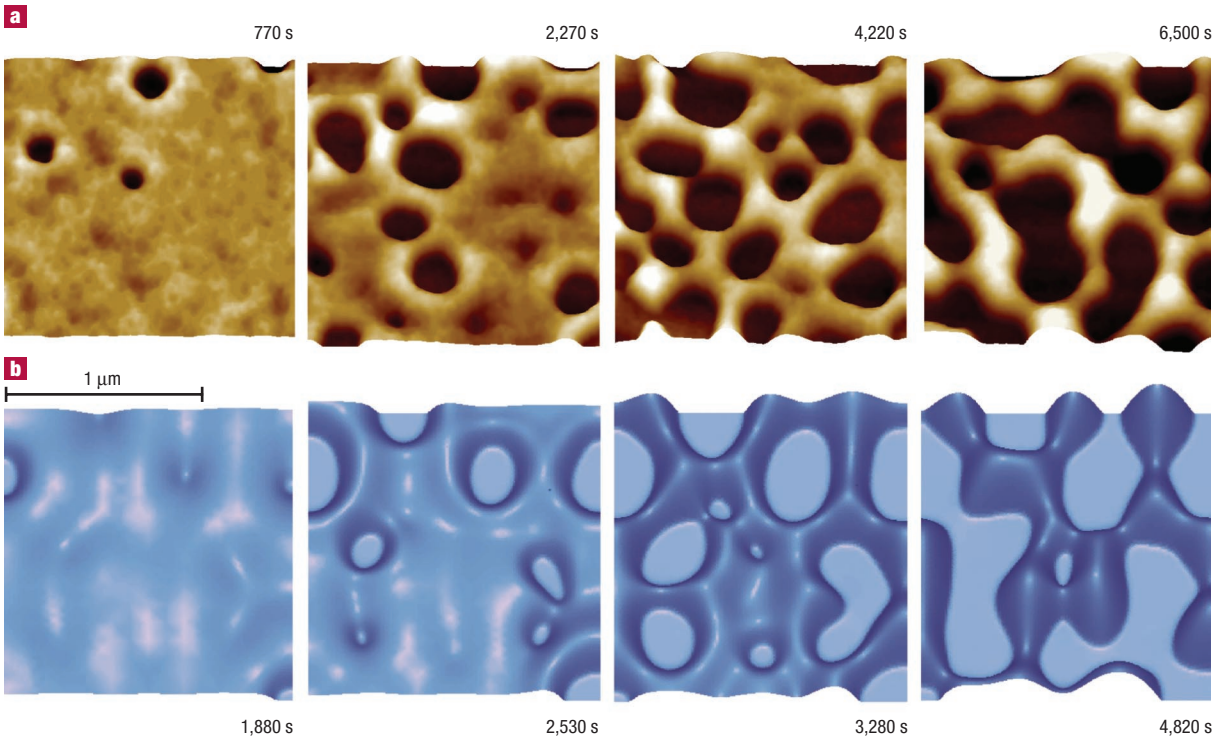

Figure 1 Dewetting morphology of a thin film. a, Experiment: Temporal series of AFM scans recorded in situ at $T = 53$ °C; a 3.9 nm PS film beads off an oxidized Si wafer. **b**, Simulated dewetting morphology with the identical system parameters as in the experiment. Highest points reach 12 nm above hole ground. The simulation started with a slightly perturbed film.

parabolic to leading order. Averaging the horizontal flow components over the vertical direction, and taking the incompressibility of the fluid into account, the following evolution equation[4] is established for h,

$$\eta \partial_t h - \nabla \cdot (m(h) \nabla p) = 0 \qquad (2)$$

Here, η is the viscosity, t is time and the augmented Laplace pressure is given by $p = -\sigma \Delta h + V'(h)$, where the prime here and later denotes differentiation of a function with respect to its argument. Finally, $m(h)$ is a non-negative mobility coefficient, which vanishes for $h = 0$ and depends on the boundary conditions of the liquid flow at the substrate—for example, no-slip entails[5] $m(h) = (h^3/3)$.

The thin-film equation (2) has a number of peculiar properties that make the design of efficient numerical schemes a challenging task. First, despite the lack of a maximum principle, globally non-negative solutions exist[6–8]—a novelty in the theory of fourth-order parabolic equations. This is due to the degeneracy of $m(h)$ in zero, and therefore the arising nonlinearities have to be discretized in a subtle way to let their impact on the qualitative behaviour carry over to the qualitative behaviour of discrete solutions. Second, the destabilization of thin liquid films can be divided into various phases evolving on vastly different timescales, characterizing, for example, film rupture, droplet formation and coarsening. Consequently, adaptivity of the numerical scheme with respect to time becomes highly desirable. Moreover, reliable information about morphology and macroscopic contact angles affords a proper tracking of moving contact lines. Altogether, it is natural to require a good numerical scheme to comply with the following catalogue: (i) non-negativity of discrete solutions; (ii) low numerical cost; (iii) convergence in all physically relevant space dimensions; (iv) precise resolution of the morphology and precise tracking of moving contact lines and free boundaries. To accomplish this, the numerical scheme used here[9,10] is inspired both by the analysis in the continuous setting and by the physics to be modelled (see Methods: Simulation).

The comparison of the results of our simulations with experiment is shown in Figs 1 and 2. Fig. 1a and 2a display atomic force microscopy (AFM) scans taken *in situ* of liquid PS films beading off an oxidized Si wafer (oxide layer thickness of 191 nm) (see Methods: Experiment). The effective interface potential for this system can be written as[2,11]

$$V(h) = \frac{\varepsilon}{h^8} - \frac{A_{SiO}}{12\pi h^2} \qquad (3)$$

where ε denotes the strength of the short-range part of the potential, $\varepsilon = 6.3(1) \times 10^{-76}$ Jm^6, and A_{SiO} is the Hamaker constant of PS on SiO, $A_{SiO} = 2.2(4) \times 10^{-20}$ J (the number in parentheses always denotes the error in units of the last digit). Note that retardation effects giving rise to a correction term proportional to h^{-3} in equation (3) are negligible. The location of the global minimum in $V(h)$ was determined by X-ray reflectometry to lie at $h = 1.3(1)$ nm, reflecting the equilibrium thickness of a PS film on top of the SiO wafer. Equation (3) serves as input into equation (2), together with the experimental parameters[12] for the (temperature-dependent) viscosity $\eta = 12{,}000$ Pa s (Fig. 1) and $\eta = 1{,}200$ Pa s (Fig. 2) and the surface tension $\sigma = 30.8$ mN m^{-1}. We note that equation (3) is a faithful representation of the interactions of our system without fitting parameters.

The difference between Figs 1 and 2 solely arises from the choice of the initial height of the film. In Fig. 1, the film is 3.9(1) nm thick, whereas in Fig. 2, it is 4.9(1) nm thick[12]. In both cases the system has a long-wave instability (spinodal dewetting)[13–22], but in the thicker film, dewetting by heterogeneous nucleation of holes pre-empts the onset of the instability[2,23]. The resulting differences in the dynamical evolution of film rupture are clearly discernible by comparison of Figs 1 and 2. In Fig. 1,

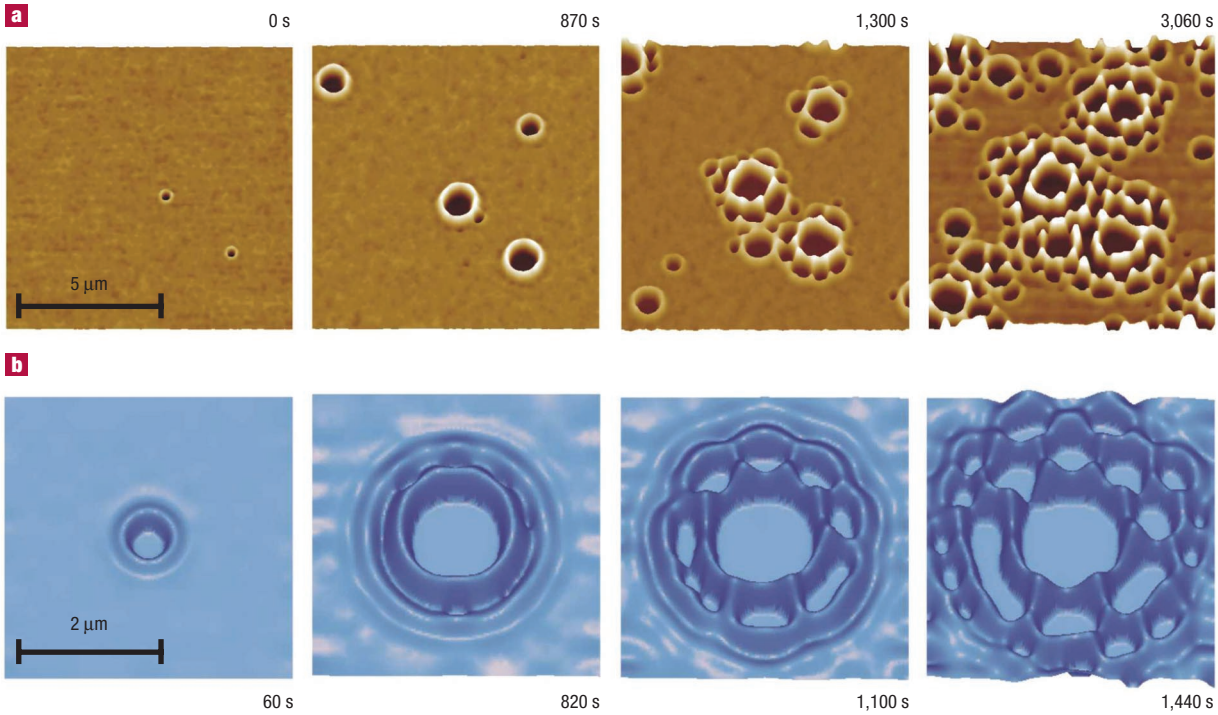

Figure 2 Satellite holes. a, Experimental dewetting scenario of a 4.9 nm PS film on an oxidized Si wafer; temporal series of AFM scans recorded in situ at $T = 70$ °C. **b**, Simulated scenario for a system with identical properties as in the experiment. Highest points reach 12 nm above hole ground. As initial data we took a slightly corrugated film with a depression in its centre.

the film surface is seen to develop a correlated pattern of indentations, whereas in Fig. 2, uncorrelated holes appear that rapidly grow in size. Owing to mass conservation, the material removed from the inner side of a hole is accumulated at the boundary of the hole, with a film depression developing behind this rim[24]. Figure 2 shows a novel pattern-formation process during dewetting: from a certain size of the first hole onwards, a second row of holes ('satellite holes') appears in this film depression, followed by a third one and so on, in a kind of hole-forming cascade. It is worth mentioning that preliminary non-dimensionalized numerical results on cascadic dewetting have been presented[22]. However, it must be emphasized that the snapshots to be found in that work (see, for example, Figure 5 in ref. 22) show holes of rectangular shape. This is at variance with our experimental findings, and it would be astonishing if this peculiarity were not a consequence of their numerical method being based on central differencing and hence rectangular grids.

We note that, for both scenarios of film rupture, our results in simulation and experiment are in close qualitative and quantitative agreement. This can, for example, already be seen by looking at the timescales involved. Taking the formation of the first hole as the origin of the time axis in simulation and experiment, the absolute timescale for the appearance of, for example, connected holes in Fig. 1 or the satellite holes in Fig. 2, are of the same order of magnitude.

Although the accordance of the timescales of experiment and simulation are a first indication of the quantitative nature of our results, the precise nature of the simulation results can be demonstrated by pattern analysis based on integral geometry, which provides accurate comparison tools beyond the visual inspection of the patterns[25–27]. This is of particular relevance, because the morphology of the rupturing film has two contributions of different character: although in the AFM image, the holes are easy to identify by eye, a description of the film in between the holes requires a closer inspection. For this we have developed a novel tomographic scheme which is applicable to both the experimental and the simulation data. To characterize the surface structures we introduce contour lines given by isosurfaces $h(\vec{x}, t) = l$ where l is a fixed threshold value and t is time, and use the Minkowski functionals $s(l)$, $u(l)$, and $\kappa(l)$ to characterize the resulting set of black and white images (see Methods: Pattern analysis). These functions are sensitive to the geometry of the film surface and measure spatial features that are not visible to the eye. An unexpected finding of this mathematical analysis is that both experiments and simulations shown in Fig. 1 follow a gaussian random-field model for contours above the average film thickness at $l_0 \approx 3.9$ nm, namely $s(l) = s_0$, $u(l) = u_0 - u_2(l - l_0)^2$, and $\kappa(l) = \kappa_1(l - l_0)$. In Fig. 3 only the time-averaged normalized data are shown for clarity, but a similar good agreement between model expectation and data are found for each snapshot at any given time. Only the parameters $s_0 = t^{-\nu_s}$, $u_2 = t^{-\nu_u}$ and $\kappa_1 = t^{-\nu_\kappa}$ depend algebraically on t with exponents $2\nu_s \approx 2\nu_\kappa \approx \nu_u \approx 1.8 \pm 0.2$ over at least two decades. An excellent consistency check is provided by the ratio $Y = s_0\kappa_1/u_2 = 2/\pi^2 \approx 0.203$ (compare with Fig. 3d), which remains constant for gaussian random fields. Moreover, the expected zeros $u'(l_0) = 0$ and $\kappa(l_0) = 0$ are matched by experiments and simulations for all times. Such a gaussian random-field behaviour is not found for the data (experiments and simulations) shown in Fig. 2, because the process of satellite hole formation involves not only uncorrelated Fourier modes, but also follows a correlated deterministic structural evolution. Details will be given elsewhere (K. R. Mecke, *et al.*, unpublished results).

In conclusion, our results demonstrate the capability of the thin-film model of equation (2) to quantitatively describe the dynamical evolution of thin-film rupture. In particular, the temporal evolution of the film morphology is mimicked perfectly by our simulations without any fitting parameter over a time-interval far exceeding the initial

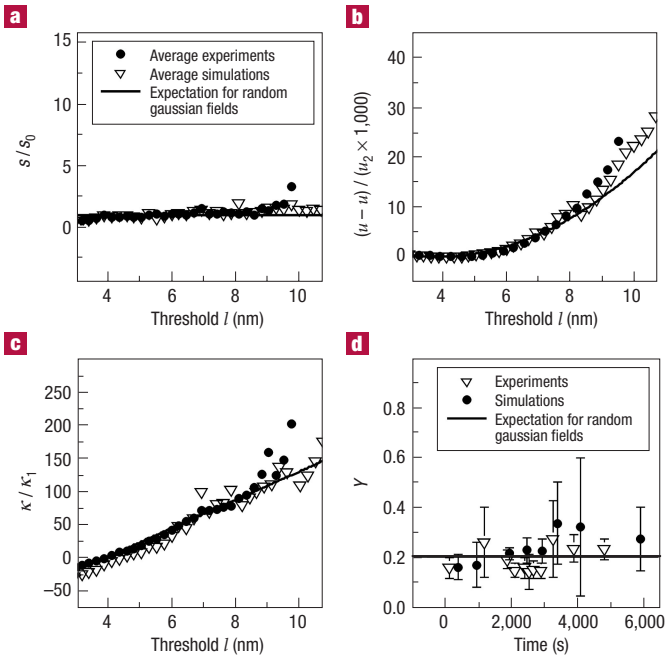

Figure 3 Analysis by Minkowski measures. Time-averaged and normalized Minkowski measures as a function of threshold value l: **a**, $s(l)$. **b**, $u(l)$. **c**, $\kappa(l)$. **d**, Ratio $Y = s_0\kappa_1/u_2$ as function of time, which is constant for gaussian fields although the values of s_0, κ_1, and u_2 change by a factor of ~100 in time. The deviations at small and large threshold values are due to nonlinearities in the dewetting process, which in principle cannot be captured by a gaussian field.

rupture event. The development of the film profiles for different complex evolution patterns can thus be monitored in both space and time. We are able to resolve fine differences in the film dynamics caused by a change in initial film thickness of only 1 nm, as observed in experiment (see Figs 1 and 2). Our pattern-analysis approach reveals that the spinodally dewetting liquid film evolves as a gaussian random field with a time-dependent variance, and allows the first quantitative characterization of the spinodal dewetting dynamics beyond the onset of the instability. Novel experimental results on a rupture process, in which deterministic events occur simultaneously with uncorrelated events, demonstrate the need for the quantitative characterization of the late-time regimes of dewetting, for which theoretical tools have not existed up to now.

The unprecedented quantitative agreement of theoretical model, experiment and simulation allows the full evolution of complex film patterns to be monitored for the first time, giving the chance to quantify the dewetting dynamics in fully nonlinear regimes—inaccessible so far to simulation or theoretical analysis. Our work will therefore have an impact on an improved understanding of thin-film dynamics and the development of thin-film technologies at nanometre scales. This is particularly relevant for the development of microfluidic devices, for example, based on the dynamics of thin, liquid films on patterned substrates[28].

METHODS

EXPERIMENT

The liquid used in our experiments was atactic PS with a molecular weight of 2 kg mol^{-1} (Polymer Labs, Church Stratton, UK, polydispersity (M_w/M_n = 1.05). This is large enough to assure non-volatility, but at the same time small enough for the polymer melt to be approximately a Newtonian fluid. This is essential for comparison with simulations, in which viscoelastic effects were neglected[29]. Films were prepared by spin-casting a toluene solution (Selectipur toluene, Merck, Germany) of PS onto polished, oxidized Si wafers (Silchem, Freiberg, Germany). Before coating, the wafers were thoroughly cleaned using standard procedures[2,11,19]. The oxide layer and PS film thickness were determined by ellipsometry (Optrel, Berlin, Germany). The surface of the wafers consists of amorphous, silicon oxide 191(1) nm thick. On such a substrate, PS films are unstable[11] up to a film thickness of about 300 nm. The symmetry-breaking mechanism of dewetting was monitored by AFM (Nanoscope III, Digital Instruments, Santa Barbara) in tapping mode. Annealing took place on top of the AFM sample holder, which enabled us to follow the dewetting process at a real timescale. We therefore continuously scanned the sample and recorded one scan every 60 s. Scanning parameters were carefully adjusted not to affect the liquid layer[11].

SIMULATION

We used a finite element method on a simplicial triangulation of the substrate, semi-implicit with respect to time, and employed linear finite elements both for the height h and the augmented Laplace pressure p. It is crucial with regard to the requirements (i)–(iii) described above, that all the integral estimates known in the continuous setting carry over to the discrete setting. In that case the analysis used in the continuous setting can be mimicked in the discrete setting. This translates to the question of how to discretize the nonlinear term $m(h)$ on each element E. Surprisingly, all the integral estimates necessary for the analysis can be retained if we replace the scalar-valued mobility $m(h)$ in the discrete setting on each finite element E by a symmetric, positive semi-definite mobility matrix[9] $M(H)$. Its eigenvalues are given by certain harmonic integral averages involving the scalar function $m(h)$ and the values of the discrete solution H in the vertices of E. Fortunately, explicit simple formulae are available to determine the coefficients of these discrete mobility matrices. As a consequence, the numerical cost compared to previous approaches is drastically reduced[9], and discrete solutions share the non-negativity properties of the corresponding solutions in the continuous setting. In particular, it is the only numerical scheme for which convergence in all the physically relevant space dimensions could be rigorously proved[10]. Finally, to guarantee a precise resolution of the morphology and of moving contact lines and to further lower the numerical cost, the scheme is adaptive both in space and in time. The time-increment was chosen to be proportional to the ratio of grid size and the spatial maximum of the vertically averaged velocity of the horizontal flow, the latter of which is of the same order as $|M(H)\nabla P|/H$ (where P is discrete pressure). The refinement of the spatial grid is controlled by ad hoc methods involving the moduli of spatial gradients. Design and numerical analysis of algorithmic concepts[9,10,30–33] for the thin-film equation as well as the simulation of dewetting processes[20–22,33] have been a topic of intensive research during the past five years. To the best of our knowledge the scheme developed in refs 9 and 10, and used for the simulations presented here, is the only one that complies with the all requirements formulated in the main text.

PATTERN ANALYSIS

Minkowski functionals $M_\nu(A)$ of domains (patterns) A in d dimensions can be defined as integrals over the boundary ∂A, $M_\nu(A) = \int_{\delta A} d\vec{x}\, C_\nu(\vec{x})$ with, for instance, in two dimensions $C_0(\vec{x}) = \vec{x}\cdot\vec{n}/2$ where $\vec{n}$ is the normal vector at the boundary point $\vec{x}\in\partial A$, and $C_1(\vec{x}) = 1$, and $C_2(\vec{x})$ denote the curvature[25]. The measures $M_\nu(A)$ of a threshold image A are related to familiar morphological quantities of area $F(l) = M_0$, boundary length $U(l) = M_1$, and Euler characteristic $\chi(l) = M_2$ of the domains where the height $h>l$ exceeds the threshold l. For convenience, we define an effective slope $s(l) = -F'(l)/U(l)$ of the height h, a logarithmic length $u(l) = \ln U(l)$ and an effective curvature $\kappa(l) = \chi(l)/U(l)$. Owing to the additivity of the Minkowski functionals this calculus is convenient for digitized data of experimental and simulation results alike: only a sum over weighted pixels has to be performed which is fast and robust[26]. Such a morphological analysis of patterns has successfully been applied before to such diverse phenomena as chemical reactions[27], liquid film rupture[19], and the distribution of galaxies in the universe (for a review, see ref. 25). Our application of Minkowski functionals is the first, to our knowledge, for gaussian random field processes in a condensed matter system.

Received 1 October 2002; accepted 11 October 2002; published 15 December 2002.

References

1. Kagan, C. R., Mitzi, D. B. & Dimitrakopoulos, C. D. Organic-inorganic hybrid materials as semiconducting channels in thin-film field-effect transistors. *Science* **286,** 945–947 (1999).
2. Seemann, R., Herminghaus, S. & Jacobs, K. Dewetting patterns and molecular forces: a reconcialiation. *Phys. Rev. Lett.* **86,** 5534–5537 (2001).
3. Acheson, D. J. *Elementary Fluid Dynamics* (Oxford Univ. Press, Oxford, 1990).
4. Oron, A., Davis, S. & Bankoff, S. G. Long-scale evolution of thin liquid films. *Rev. Mod. Phys.* **69,** 931–980 (1997).
5. Dussan V, E. B. & Davis, S. On the motion of a fluid-fluid interface along a solid surface. *J. Fluid. Mech.* **65,** 71–95 (1974).
6. Bernis, F. & Friedman, A. Higher order nonlinear degenerate parabolic equations. *J. Differ. Equations* **83,** 179–206 (1990).
7. Dal Passo, R., Garcke, H. & Grün, G. On a fourth order degenerate parabolic equation: global entropy estimates and qualitative behavior of solutions. *SIAM J. Math. Anal.* **29,** 321–342 (1998).
8. Bertozzi A. L. & Pugh, M. The lubrication approximation for thin viscous films: regularity and long time behaviour of weak solutions. *Comm. Pure Appl. Math.* **49,** 85–123 (1996).
9. Grün, G. & Rumpf, M. Nonnegativity preserving convergent schemes for the thin film equation. *Num. Math.* **87,** 113–152 (2000).
10. Grün, G. On the convergence of entropy consistent schemes for lubrication type equations in multiple space dimensions. *Math. Comp.* (in the press).
11. Seemann, R., Herminghaus, S. & Jacobs, K. Gaining control of pattern formation of dewetting liquid films. *J. Phys. Condens. Mat.* **13,** 4925–4938 (2001).
12. Herminghaus, S., Seemann, R. & Jacobs, K. The glass transition of thin polymer films: some questions and a possible answer. *Eur. Phys. J.* E **5,** 531–538 (2001).
13. Vrij, A. Possible mechanism for the spontaneous rupture of thin, free liquid films. *Discuss. Faraday Soc.* **42,** 23–33 (1966).
14. Ruckenstein E. & Jain, R. K. Spontaneous rupture of thin liquid films. *J. Chem. Soc. Faraday Trans. II* 132–147 (1974).
15. Brochard, F. & Daillant, J. Drying of solids wetted by thin liquid films. *Can. J. Phys.* **68,** 1084–1088 (1990).

16. Reiter, G. Dewetting of thin polymer films. *Phys. Rev. Lett.* **68,** 751–754 (1992).
17. Bischof, J., Scherer, D., Herminghaus, S. & Leiderer, P. Dewetting modes of thin metallic films: nucleation of holes and spinodal dewetting. *Phys. Rev. Lett.* **77,** 1536–1539 (1996).
18. Jacobs, K., Mecke, K. R. & Herminghaus, S. Thin liquid polymer films rupture via defects. *Langmuir* **14,** 965–969 (1998).
19. Herminghaus, S. *et al.*, Spinodal dewetting in liquid crystal and liquid metal films. *Science* **82,** 916–919 (1998).
20. Sharma, A. & Khanna, R. Pattern formation in unstable liquid films. *Phys. Rev. Lett.* **81,** 3463–3466 (1998).
21. Ghatak, A., Khanna, R. & Sharma, A. Dynamics and morphology of holes in dewetting of thin films. *J. Colloid Interface Sci.* **212,** 483–494 (1999).
22. Kargupta, K. & Sharma, A. Creation of ordered patterns by dewetting of thin films on homogeneous and heterogeneous substrates. *J. Colloid Interface Sci.* **245,** 99–115 (2002).
23. Blossey, R. Nucleation at first-order wetting transitions. *Int. J. Mod. Phys. B* **9,** 3489–3525 (1995).
24. Seemann, R., Herminghaus, S. & Jacobs, K. Shape of a liquid front upon dewetting. *Phys. Rev. Lett.* **81,** 1251–1254 (2001).
25. Mecke, K. R. Integral geometry and statistical physics. *Int. J. Mod. Phys. B* **12,** 861–899 (1998).
26. Mecke, K. R. & Stoyan, D. (eds.) *Statistical Physics and Spatial Statistics - The Art of Analysing and Modelling Spatial Structures and Pattern Formation* Lecture Notes in Physics, Vol. 554, (Springer, Berlin, 2000).
27. Mecke, K. R. Morphological characterization of patterns in reaction-diffusion systems. *Phys. Rev. E* **53,** 4794–4800 (1996).
28. Gau, H., Herminghaus, S., Lenz, P. & Lipowsky, R. Liquid morphologies on structured surfaces. *Science* **283,** 46–49 (1999).
29. Herminghaus, S., Seemann, R. & Jacobs, K. Generic morphologies of viscoelastic dewetting fronts. *Phys. Rev. Lett.* **89,** 056101 (2002).
30. Barrett, J. W., Blowey, J. F. & Garcke, H. Finite element approximation of a fourth order nonlinear degenerate parabolic equation. *Num. Math.* **80,** 525–556 (1998).
31. Zhornitskaja, L. & Bertozzi, A. L. Positivity preserving numerical schemes for lubrication-type equations. *SIAM J. Num. Anal.* **37,** 523–555 (2000).
32. Grün, G. & Rumpf, M. Simulation of singularities and instabilities in thin film flow. *Europ. J. Appl. Math.* **12,** 293–320 (2001).
33. Oron, A. Three-dimensional nonlinear dynamics of thin liquid films. *Phys. Rev. Lett.* **85,** 2108–2111 (2000).

Acknowledgements

We thank Stephan Herminghaus for many stimulating discussions and Renate Konrad for help in calculating the Minkowski measures. This work was supported by the Priority Program *Wetting and Structure Formation at Interfaces* of the German Science Foundation through individual research grants to the participating groups. This program provided an ideal forum for the interaction of mathematicians, theoretical and experimental physicists which lead to this interdisciplinary work.
Correspondence and requests for materials should be addressed to R.B.

Competing financial interests

The authors declare that they have no competing financial interests.